Majorana phase gate based on the geometric phase

Andrzej Więckowski [*], Marcin Mierzejewski [†], and Michał Kupczyński [‡]

*Department of Theoretical Physics, Faculty of Fundamental Problems of Technology, Wrocław University of Science and Technology,
PL-50370 Wrocław, Poland*

We study the dynamics of a single qubit encoded in two pairs of Majorana modes, whereby each pair is hosted on a trijunction described by the Kitaev model extended by many-body interactions. We demonstrated that the challenging phase gate may be efficiently implemented via braiding of partially overlapping modes. Although such a qubit acquires both geometric and dynamical phases during the braiding protocol, the latter phase may be eliminated if the Majorana modes are hosted by systems with appropriate particle-hole symmetry.

I. INTRODUCTION

The Majorana zero-energy modes (MZMs) have recently attracted significant interest as building blocks of future topological quantum computers [1–11]. So far, experimental and theoretical studies have focused mostly on finding an optimal physical system that hosts the MZM [12–18] as well as on developing appropriate techniques which clearly confirm the existence of MZMs therein [19–21]. Recent experimental results strongly support the presence of the MZM in superconductor-semiconductor hybrid nanostructures [22–31], in one-dimensional monoatomic chains deposited on the surface of superconductors [32–37], in the superconducting vortices [38–41], and in two-dimensional topological superconductors [42,43].

The fundamental problem for quantum computing is to effectively implement the set of universal gates which consists of the Hadamard gate, the Z gate, and also the $\pi/8$ gate (phase gate) [44]. The general scheme for building the former two gates is already well established via topologically protected braiding operations of MZMs [45–56]. However, the phase gate poses a challenging problem since the latter operations are insufficient for its implementation [6]. The very basic method of overcoming this problem is to bring two Majorana quasiparticles close to each other [6]. The MZMs are operators which map an eigenstate from one parity sector to a state in another sector with identical energy. Bringing two MZMs together lifts the latter degeneracy (MZMs are no longer strict zero modes) and splits the levels for odd and even numbers of particles by δE. In principle, the phase shift needed for the phase gate can be obtained via fine tuning of two parameters: δE and the period of time Δt for which the MZMs are brought close to each other. However, the resulting phase is not protected by any symmetry, and as a consequence, each such operation must be followed by an error correction, e.g., via the magic state distillation [57].

The phase shift induced via the proximity of two MZMs is a dynamical phase. Such an operation requires precise control of two independent parameters: δE and Δt. In the present work we derive another possibility in which fine tuning of Δt is eliminated. It consists of double braiding two MZMs, which were previously brought together, so that the Majorana edge states partially overlap in the real space. Braiding of such overlapping modes leads to a small shift of the *geometric phase* with respect to results for spatially separated MZMs [53]. The geometric phase is independent of the braiding time Δt; hence, it is better suited for building the phase gate than the simple protocol based on the dynamical phase. Despite the apparent advantage of such a protocol, an important problem remains to be solved: a qubit built out of overlapping MZMs acquires during its evolution not only the geometric phase but also the dynamical phase, where the latter occurs due to the energy splitting δE. However, we demonstrate that the dynamical phase may be effectively eliminated if the MZMs are hosted by appropriate systems with particle-hole symmetry. The latter property is shown to hold also for systems with many-body interactions. We also show that the shift of the geometric phase is connected to the spatial redistribution of MZMs. The discussed scenario is rather general and is not limited to a particular realization of the braiding protocol.

This paper is organized as follows: in Sec. II we recall the method of storing a qubit in four MZMs (sparse encoding) and specify the microscopic model of a system that hosts MZMs; next, in Sec. III we present our numerical results concerning the geometric and dynamical phases gained after braiding overlapping Majorana modes and show how the latter phase may be eliminated; finally, we summarize our results in Sec. IV.

II. MODEL AND DETAILS OF BRAIDING

We study the dynamics of a single qubit (sparsely) encoded in two pairs of MZMs, Γ_1, Γ_2 and Γ_3, Γ_4. Each pair of MZMs is hosted on a trijunction schematically shown in Fig. 1(a), whereas the entire system is sketched in Fig. 2. The basis of the qubit consists of two states with an even total number

---

[*]andrzej.wieckowski@pwr.edu.pl
[†]marcin.mierzejewski@pwr.edu.pl
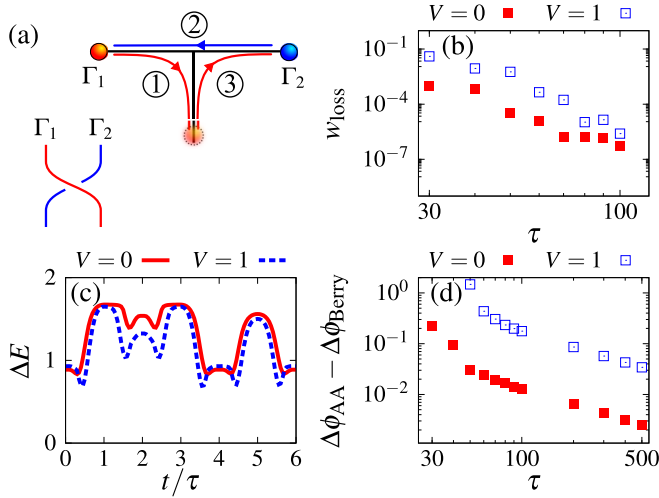[‡]michal.kupczynski@pwr.edu.pl

014504-1

FIG. 1. (a) Sketch of a trijunction hosting a pair of MZMs, Γ_1 and Γ_2, as well as the braiding procedure marked schematically with arrows, (b) loss of the fidelity w_{loss} as a function of the total evolution time $T = 6\tau$, (c) energy gap ΔE vs time t/τ, and (d) difference between $\Delta\phi_{\text{AA}}$ and $\Delta\phi_{\text{Berry}}$ vs the evolution time $T = 6\tau$. Results are for a system with ($V = 1$) and without ($V = 0$) many-body interactions (see labels) for $L = 7$, $\Delta = 0.8$, $\mu = 0$.

of fermions, $|0\rangle = |e_{12}\rangle \otimes |e_{34}\rangle$ and $|1\rangle = |o_{12}\rangle \otimes |o_{34}\rangle$. Here, $|e_{12}\rangle$ and $|o_{12}\rangle$ denote the states of the junction J_{12} with even and odd numbers of fermions, respectively. Similar notation holds for junction J_{34}.
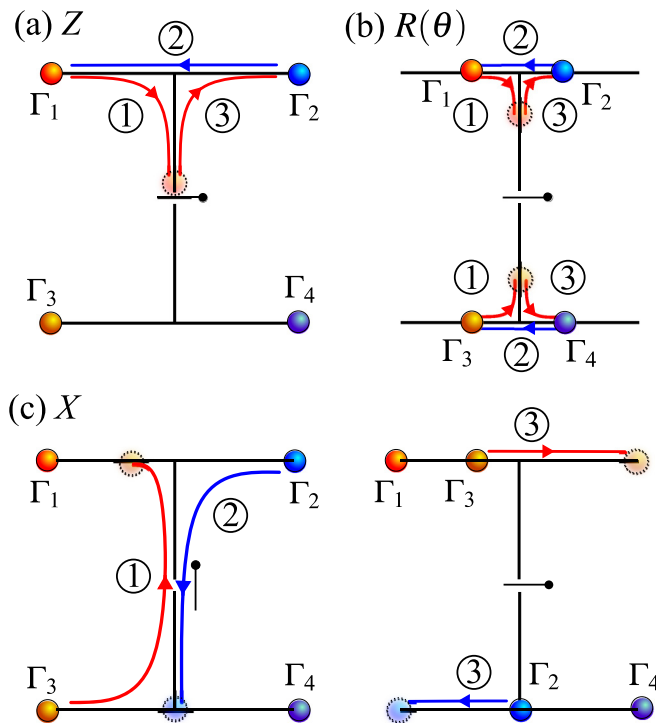

FIG. 2. Two connected trijunctions forming Majorana qubit consisting of four MZMs: Γ_1, Γ_2, Γ_3, Γ_4. As discussed in Sec. III F, the double execution of the sketched protocols is equivalent to (a) the Z gate, (b) $R(\theta)$ phase gate, and (c) X gate.

We study the simplest setup which allows for the braiding of MZMs [45,53]. Namely, we consider a trijunction [see Fig. 1(a)] consisting of three chains of equal length, and we set for each chain a different phase of the superconducting order parameter, $\Delta_{ij} = \Delta \exp(-i\varphi_{ij})$, where $\varphi_{ij} = 0$, $+\frac{\pi}{2}$, $-\frac{\pi}{2}$ in the left, right, and vertical chains, respectively. We assume also that each junction contains L sites and is described by the Kitaev model [58] with many-body interaction,

$$H(t) = H_0 + \sum_i \mu_i(t)\widetilde{n}_i,$$

$$H_0 = \sum_{\langle i,j\rangle}[(t_0 a_i^\dagger a_j + \Delta_{ij} a_i^\dagger a_j^\dagger) + \text{H.c.} + V\,\widetilde{n}_i\widetilde{n}_j]. \quad (1)$$

Here, $a_i^\dagger$ creates a fermion on site i, $\widetilde{n}_i = a_i^\dagger a_i - \frac{1}{2}$, t_0 is the hopping between the neighboring sites on a junction, and V is the nearest-neighbor repulsion.

The time dependence of $\mu_i(t)$ allows us to implement the braiding of MZMs, as described below in more detail. We use dimensionless units, $\hbar = 1$ and $t_0 = 1$. The motivation for introducing the many-body interaction is that we study a quasi-one-dimensional system, where even weak Coulomb interactions may significantly affect the properties of the system. In particular, in the absence of superconductivity, the wires are described by the interacting Luttinger liquids [59]. The Majorana states are not completely immune against many-body interactions [60–67], whereas moderate interactions may even stabilize the MZMs [68–71].

In the case of a single Kitaev chain with a uniform and time-independent $\mu_i(t) = \mu$, one may switch between the trivial and the topological phases via tuning the chemical potential. In a system without many-body interaction ($V = 0$) and nonzero $|\Delta| > 0$, the topological phase is present for $|\mu| \leqslant 2t_0$, while the trivial one is present for $|\mu| > 2t_0$ [58,72]. The topological regime in a system with many-body interaction was discussed, e.g., in [62,63,73]. The braiding is achieved via slow tuning of $\mu_i(t)$ in such a way that selected sites remain in the topological regime, whereas the others remain in the trivial regime [45]. Namely,

$$\mu_i(t) = \mu_c g_i(t) + \mu, \quad (2)$$

where μ is the uniform chemical potential and we set $\mu_c = \pm 4$. The details of the ramping protocol, $g_i(t) \in [0, 1]$, are the same as in Ref. [53] and are recalled in the Appendix.

The braiding protocol describes a cyclic evolution of the Hamiltonian (1) in the parameter space. The many-body wave function is obtained from the numerical solution of the time-dependent Schrödinger equation $i\partial_t|\psi(t)\rangle = H(t)|\psi(t)\rangle$, where $|\psi(0)\rangle$ is the ground state of the initial Hamiltonian $H(0)$. The ground state has been obtained from the Lanczos method, studying independently sectors with odd and even particle numbers. The evolution $|\psi(t)\rangle \rightarrow |\psi(t + \delta t)\rangle$ is calculated in small time windows, $\delta t \sim 0.01$, by expanding the unitary propagators $\exp[-iH(t + \delta t/2)\delta t]$ in the Chebyshev polynomials [74–76].

First, we consider a single braiding of two MZMs on a single trijunction, as shown in Figs. 1(a) and 2(a). Initially ($t = 0$), we set $\mu_i = \mu_c$ for sites i in the vertical chain, which is then in the trivial regime. Two remaining (horizontal) chains are in the topological regime and host two MZMs located

at the edges of these wires. Next, by adiabatic tuning of $g_i(t)$, we control the boundaries of the topological regime and swap the positions of Γ_1 and Γ_2 [see Fig. 1(a)]. We split our protocol into six equal time windows: $(0, \tau)$, moving Γ_1 to the center of the junction; $(\tau, 2\tau)$, moving Γ_1 to the edge of the vertical chain; $(2\tau, 3\tau)$, moving Γ_2 to the center of the junction; $(3\tau, 4\tau)$, moving Γ_2 to the edge of the left chain; $(4\tau, 5\tau)$, moving Γ_1 to the center of the junction; and $(5\tau, 6\tau)$, moving Γ_1 to the edge of the right chain. These steps are shown explicitly in Fig. 8, presented in the in the Appendix.

III. RESULTS

A. Geometric phase for braiding on a single trijunction

We examine the non-Abelian properties of MZMs by calculating the geometric phases: the Berry phase ϕ_{Berry} in the case of the adiabatic evolution [77] and the Aharonov-Anandan phase ϕ_{AA} in the case of a general cyclic evolution [78]. However, first, we check when the evolution is cyclic, i.e., when the final quantum state $|\psi(T)\rangle\langle\psi(T)|$ equals the initial one $|\psi(0)\rangle\langle\psi(0)|$, where for the present protocol $T = 6\tau$. We examine this property by calculating the loss of the fidelity,

$$w_{\text{loss}} = 1 - |\langle\psi(T)|\psi(0)\rangle|^2, \quad (3)$$

which is shown in Fig. 1(b). One may observe that this quantity decreases when the evolution time increases and becomes negligible for $\tau \gtrsim 100$. The necessary condition for the adiabaticity of the time evolution is a nonvanishing energy gap between the ground state and the first excited state. In Fig. 1(c) we show the gap $\Delta E = \min\{E_1^o - E_0^o, E_1^e - E_0^e\}$ during the entire evolution, where $E_n^{e(o)}$ is the energy of the n eigenstate in the even- (odd-) parity sector. Since ΔE does not vanish, the evolution should be adiabatic for sufficiently large τ.

In the case of a cyclic evolution the initial and final wave functions differ only by the phase factor,

$$|\psi(T)\rangle = e^{i\phi}|\psi(0)\rangle = e^{i(\phi_{\text{dyn}}+\phi_{\text{geo}})}|\psi(0)\rangle, \quad (4)$$

which contains both the gauge-invariant geometric phase ϕ_{geo} and the dynamical phase ϕ_{dyn} [79]. We evaluate the geometric phase from the standard expression [80],

$$\phi_{\text{geo}} = \arg[\langle\psi(0)|\psi(T)\rangle] - \arg\left[\prod_{j=0}^{N-1}\langle\psi(t_j)|\psi(t_{j+1})\rangle\right], \quad (5)$$

where $t_0 = 0$ and $t_N = T$. In the case of a generic cyclic quantum evolution, ϕ_{geo} evaluated from Eq. (5) represents ϕ_{AA}. Then, the wave function $|\psi(t_j)\rangle$ is obtained directly from the time-dependent Schrödinger equation. In the case of the adiabatic cyclic evolution, $\phi_{\text{AA}} = \phi_{\text{Berry}}$. Then, the wave functions $|\psi(t_j)\rangle$ are obtained from the diagonalization of the instantaneous Hamiltonians $H(t_j)$.

The essential quantity for implementing the Majorana quantum gates is the difference between phases acquired during evolution in sectors with even and odd particle numbers: $\Delta\phi_{\text{geo}} = \phi_{\text{geo}}^e - \phi_{\text{geo}}^o$, (see the basis states of the qubit). As a final test of the adiabatic evolution, in Fig. 1(d) we show that the difference $\Delta\phi_{\text{AA}} - \Delta\phi_{\text{Berry}}$ decreases with increasing τ.

The latter difference is significantly larger for systems with many-body interactions; nevertheless, one may expect that it vanishes for $\tau \to \infty$ also for $V \neq 0$. Therefore, from now on we focus only on the adiabatic evolution.

Finally, we introduce the dynamical phase for the adiabatic evolution in the ground states, e.g., for $|e_{12}(t)\rangle$:

$$\phi_{\text{dyn}}^{e,J_{12}} = \int_0^T dt\, \langle e_{12}(t)|H(t)|e_{12}(t)\rangle, \quad (6)$$

and the phase difference between even- and odd-parity sectors,

$$\Delta\phi_{\text{dyn}}^{J_{12}} = \phi_{\text{dyn}}^{e,J_{12}} - \phi_{\text{dyn}}^{o,J_{12}}. \quad (7)$$

The latter quantity is proportional to the difference of the ground-state energies in various sectors, $\delta E = E_0^e - E_0^o$. One tries to eliminate the dynamical phase and work only with the geometric phase.

If Majorana fermions are separated in real space, then they are strict zero modes; hence, $E_0^e = E_0^o$, and $\Delta\phi_{\text{dyn}}^{J_{12}} = 0$. Then, the only contribution to the phase difference comes from the geometric phase, $\Delta\phi = \Delta\phi_{\text{Berry}}$. It is well established that the braiding of strict MZMs leads to $\Delta\phi_{\text{Berry}} = \pm\frac{\pi}{2}$ [45]. In order to construct the phase gate based on the geometric phase, one needs a protocol for which $\Delta\phi_{\text{Berry}} = \pi/4$ [44], whereas $\Delta\phi_{\text{dyn}} = 0$. Such a gate is unprotected by topology, but it is adiabatic; that is, the acquired phase is independent of the evolution time.

B. Braiding error due to overlap of the Majorana fermions

The geometric phase is a gauge-invariant quantity provided that the Hamiltonian follows a closed loop in the parameter space. However, in order to gain more insight, we introduce also the adiabatic *exchange phase* $\Delta\varphi_{\text{ex}}(t)$, defined for arbitrary $0 \leqslant t \leqslant T$ [53], such that $\Delta\phi_{\text{Berry}} = \Delta\varphi_{\text{ex}}(T)$. Figure 3(a) shows the latter quantity. While the exchange phase
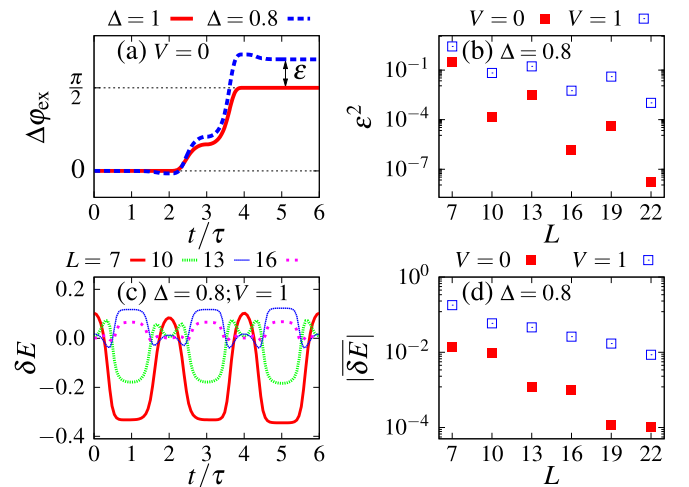

FIG. 3. Single braiding on a single trijunction for $\mu = 0$: (a) exchange phase $\Delta\varphi_{\text{ex}}$ during evolution as a function of time t/τ for $L = 7$, (b) finite-size scaling of the braiding error ε, (c) split between the instantaneous ground-states energies in different parity sectors $\delta E(t) = E_0^e(t) - E_0^o(t)$, and (d) finite-size scaling of the average energy split δE.

is not gauge invariant and could depend on the particular realization of a protocol, it gives intuitive insight into the details of the protocol [50,53,81]. For the special case $\Delta = 1$, $V = 0$, the MZMs are located on single edge sites and do not overlap during the braiding even for a finite system. Then, $\Delta\phi_{\text{Berry}} = \frac{\pi}{2}$ for arbitrary L, as shown in Fig. 3(a). However, for $\Delta \neq 1$ and finite L, such a phase deviates from $\frac{\pi}{2}$ by a braiding error, $\varepsilon = \Delta\phi_{\text{Berry}} - \frac{\pi}{2}$. Figure 3(b) demonstrates that the braiding error is a finite-size effect. In the case of an infinite trijunction, when the MZMs are fully separated in real space, ε seems to vanish, and the Berry phase equals $\frac{\pi}{2}$.

We stress that a nonzero braiding error is intimately connected to a nonvanishing dynamical phase. Overlap of the Majorana fermions lifts the degeneracy of the ground state, $E_0^e \neq E_0^o$; hence, in general, $\Delta\phi_{\text{dyn}}^{J_{12}} \neq 0$. The energy splitting δE depends on the distance between the Majorana fermions, which varies during the evolution. In Fig. 3(c) we show the instantaneous δE as a function of the evolution time t/τ for different system sizes L. It is clear that δE decreases when L increases. In order to discuss this effect in more detail, we have calculated the average splitting $\overline{\delta E} = \frac{1}{T}\int_o^T dt\, \delta E(t)$, which also determines the dynamical phase $\Delta\overline{\phi}_{\text{dyn}}^{J_{12}} = T\overline{\delta E}$. Figure 3(d) shows the finite-size scaling of $\overline{\delta E}$, which seems to decay almost exponentially with increasing L.

C. Cancelation of the dynamical phases

While the braiding error should be avoided in the topologically protected operations, it may still be very useful for constructing the phase gate with arbitrary phase shift. The advantage of such a solution over the simplest protocol based on getting Majorana fermions close to each other consists of the fact that $\Delta\phi_{\text{Berry}}$ does not depend on the total evolution time T. However, a nonzero braiding error is intimately connected to a nonzero dynamical phase. Therefore, the idea of using the Berry phase would be useless unless one finds a method of eliminating the dynamical phase. Below we show that $\Delta\phi_{\text{dyn}}$ can, indeed, be eliminated by appropriate tuning of junctions which build the Majorana qubit.

We assume that both trijunctions, J_{12} and J_{34}, are described by the same Hamiltonian (1), which is particle-hole symmetric up to the term containing μ_i [see Eq. (2)]. Each junction contains an *odd* number of sites, and the braiding is applied *twice* to each junction [see Fig. 2(b)]. However, one applies positive μ_i for one junction and negative μ_i for the other. Namely, the trijunctions J_{12} and J_{34} are described, respectively, by the Hamiltonians

$$H_{12}(\Delta_{ij}) = H_0(\Delta_{ij}) + \sum_i \mu_i(t)\widetilde{n}_i, \quad (8)$$

$$H_{34}(\Delta_{ij}) = H_0(\Delta_{ij}) - \sum_i \mu_i(t)\widetilde{n}_i, \quad (9)$$

where for clarity of the present discussion we explicitly mark the dependence of Hamiltonians on the superconducting order parameter.

In Fig. 4(a) we present the geometric phase $\Delta\varphi_{\text{ex}}$ gained by each junction during such a double-braiding protocol. The sign of μ_i does not influence the geometric phase, and we find $\Delta\overline{\phi}_{\text{Berry}}^{J_{12}} = \Delta\overline{\phi}_{\text{Berry}}^{J_{34}} = \pi + 2\varepsilon$. Here, the symbol $\bar{\ }$ indicates
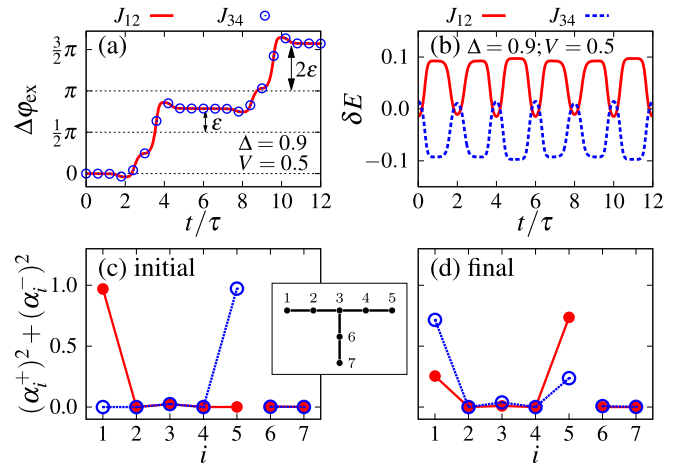

FIG. 4. (a) and (b) Double braiding for $\mu = 0$. We set $\mu_c = 4$ and $\mu_c = -4$ for junctions J_{12} and J_{34}, respectively. (a) Exchange phase $\Delta\varphi_{\text{ex}}$ and (b) energy splittings δE determined separately for each junction. Spatial structures of Majorana fermions Γ_1 (red solid line) and Γ_2 (blue dashed line) (c) before and (d) after single braiding for $\Delta = 0.8$ and $V = 0$ ($L = 7$, $\mu = 0$).

that braiding is applied twice. However, Fig. 4(b) shows that the energy splittings δE for the trijunctions J_{12} and J_{34} have opposite signs; hence, $\Delta\overline{\phi}_{\text{dyn}}^{J_{12}} + \Delta\overline{\phi}_{\text{dyn}}^{J_{34}} = 0$. In order to explain the latter identity we assume that the sites within each junction are enumerated according to the scheme shown in the inset in Fig. 4(c). Then, it is easy to check (for odd L) that the neighboring sites $\langle i, j \rangle$ are labeled by integers with opposite parities; that is, if i is odd, then j is even. In other words, the trijunctions form a bipartite lattice consisting of two sublattices which contain, respectively, odd and even lattice sites i.

We consider a standard particle-hole (Shiba) transformation [82],

$$U = (a_L^\dagger - a_L)(a_{L-1}^\dagger + a_{L-1})\cdots(a_2^\dagger + a_2)(a_1^\dagger - a_1), \quad (10)$$

for which $U^\dagger U = UU^\dagger = 1$ and $U a_i U^\dagger = (-1)^i a_i^\dagger$. One finds that Hamiltonians of both junctions are connected via this particle-hole transformation,

$$UH_{12}(\Delta_{ij})U^\dagger = H_{34}(\Delta_{ij}^*), \quad (11)$$

whereas the parity operator

$$P = \prod_{i=1}^L (1 - 2a_i^\dagger a_i) \quad (12)$$

is odd under the latter transformation, $UPU^\dagger = (-1)^L P = -P$. Considering an eigenstate $|n\rangle$ of $H_{12}(\Delta_{ij})$,

$$H_{12}(\Delta_{ij})|n\rangle = E_n|n\rangle, \quad P|n\rangle = p_n|n\rangle, \quad (13)$$

one finds that $U|n\rangle$ is an eigenstate of $H_{34}(\Delta_{ij}^*)$ with energy E_n but with the opposite parity, $PU|n\rangle = -p_n U|n\rangle$. Therefore, $H_{12}(\Delta_{ij})$ and $H_{34}(\Delta_{ij}^*)$ have the same energy spectra, but with swapped parities of the energy levels. It is also clear that the energy spectrum of $H_{34}(\Delta_{ij}^*)$ is the same as that of $H_{34}(\Delta_{ij})$.

Overlapping of the Majorana fermions lifts the ground-state degeneracy; however, the above particle-hole transformation holds true during the entire quantum evolution. Then,

using Eq. (6), one finds that $\bar{\phi}_{\mathrm{dyn}}^{e,J_{12}} = \bar{\phi}_{\mathrm{dyn}}^{o,J_{34}}$ as well as $\bar{\phi}_{\mathrm{dyn}}^{o,J_{12}} = \bar{\phi}_{\mathrm{dyn}}^{e,J_{34}}$ and, consequently,

$$\Delta\bar{\phi}_{\mathrm{dyn}}^{J_{12}} + \Delta\bar{\phi}_{\mathrm{dyn}}^{J_{34}} = \bar{\phi}_{\mathrm{dyn}}^{e,J_{12}} - \bar{\phi}_{\mathrm{dyn}}^{o,J_{12}} + \bar{\phi}_{\mathrm{dyn}}^{e,J_{34}} - \bar{\phi}_{\mathrm{dyn}}^{o,J_{34}} = 0. \quad (14)$$

The phases gained by the qubit's basis states read

$$|0\rangle_{t=2T} = \exp\left[i\left(\bar{\phi}_{\mathrm{dyn}}^{e,J_{12}} + \bar{\phi}_{\mathrm{geo}}^{e,J_{12}} + \bar{\phi}_{\mathrm{dyn}}^{e,J_{34}} + \bar{\phi}_{\mathrm{geo}}^{e,J_{34}}\right)\right]|0\rangle_{t=0},$$

$$|1\rangle_{t=2T} = \exp\left[i\left(\bar{\phi}_{\mathrm{dyn}}^{o,J_{12}} + \bar{\phi}_{\mathrm{geo}}^{o,J_{12}} + \bar{\phi}_{\mathrm{dyn}}^{o,J_{34}} + \bar{\phi}_{\mathrm{geo}}^{o,J_{34}}\right)\right]|1\rangle_{t=0}; \quad (15)$$

hence, the cyclic evolution of an arbitrary state of the qubit $|\psi\rangle$ takes the form

$$|\psi(2T)\rangle = e^{i\chi} R(\theta)|\psi(0)\rangle, \quad (16)$$

where

$$R(\theta) = \begin{bmatrix} 1 & 0 \\ 0 & e^{i\theta} \end{bmatrix}, \quad |0\rangle = \begin{bmatrix} 1 \\ 0 \end{bmatrix}, \quad |1\rangle = \begin{bmatrix} 0 \\ 1 \end{bmatrix}. \quad (17)$$

Here, $R(\theta)$ is the phase gate, while χ is a global phase that is not relevant for the operation of the latter gate [44]. Using Eqs. (14) and (16), one finds

$$\chi = \bar{\phi}_{\mathrm{dyn}}^{e,J_{12}} + \bar{\phi}_{\mathrm{dyn}}^{e,J_{34}} + \bar{\phi}_{\mathrm{geo}}^{e,J_{12}} + \bar{\phi}_{\mathrm{geo}}^{e,J_{34}}, \quad (18)$$

$$\theta = -\Delta\bar{\phi}_{\mathrm{geo}}^{J_{12}} - \Delta\bar{\phi}_{\mathrm{geo}}^{J_{34}} = -4\varepsilon. \quad (19)$$

Due to the particle-hole symmetry, the operation of the gate depends solely on the braiding error for the geometric phase ($\theta = -4\varepsilon$), whereas the dynamical phases enter only the global phase.

To summarize this section, we note that the discussed scenario is general in that it is independent of the particular form of the Hamiltonian (1) and arises solely from its particle-hole symmetry. One needs to apply the same protocol to both junctions; however, the execution of these protocols does not need to be synchronized in time. In other words, the protocols can be executed on two trijunctions sequentially; however, the variations of the parameters within the same time interval must be identical for both junctions, up to the opposite signs of $\mu_i(t)$. The time dependence of $\mu_i(t)$ may be implemented by applying opposite gate voltages to both junctions. Experimental application of this protocol may still pose challenging technical problems. In particular, both junctions may not be identical, more realistic Hamiltonians may contain terms which break the particle-hole symmetry, or $\mu_i(t)$ on both junctions may have slightly different magnitudes. Then, in general, the dynamical phase would also contribute to the phase θ in Eq. (17), and the latter contribution could be eliminated only via fine tuning of the experimental setup, e.g., via tuning the execution time on one trijunction. If such fine tuning turns out to be insufficient, the protocol should be followed by the error correction [57]; however, the initial error is expected to be smaller than in the protocol based on a purely dynamical phase of overlapping Majorana modes.

D. Tuning of the geometric phase

The main result of the present work concerns the phase gate based on the braiding error ε, i.e., the deviation of the Berry phase $\Delta\phi_{\mathrm{Berry}}$ from $\frac{\pi}{2}$. The braiding error vanishes for
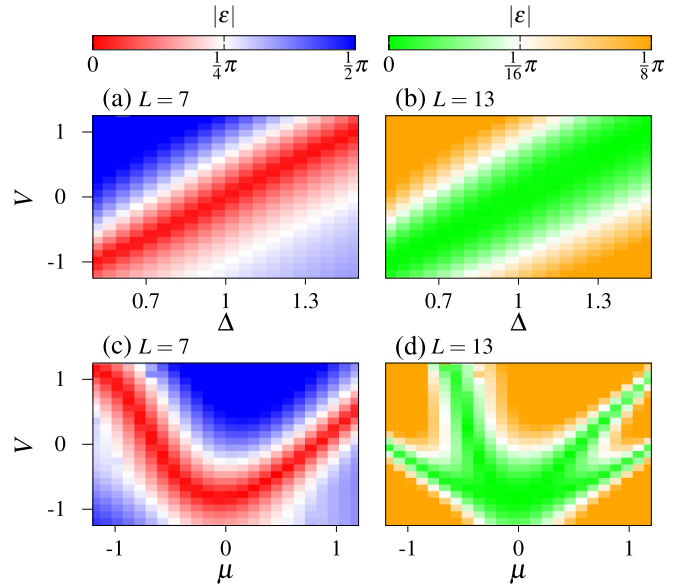

FIG. 5. Absolute value of the braiding error ε (i.e., the deviation of the Berry phase $\Delta\phi_{\mathrm{Berry}}$ from $\frac{\pi}{2}$): (a) and (b) $|\varepsilon|$ as a function of interaction V and superconducting gap Δ ($\mu = 0$) for $L = 7$ and $L = 13$, respectively, and (c) and (d) $|\varepsilon|$ as a function of interaction V and chemical potential μ ($\Delta = 0.6$) for $L = 7$ and $L = 13$, respectively.

the topologically protected gates when one braids nonoverlapping MZMs on an infinite trijunction. However, in order to construct the standard $\pi/8$ gate, one needs $\varepsilon = \pi/16$. Here, we show for a finite junction that ε may be rather easily tuned via changing the parameters of the Hamiltonian (1).

Since ε originates from the overlap of Majorana fermions, it strongly depends on the system size. Figures 5 shows $|\varepsilon|$ for $L = 7$ and $L = 13$, which are the smallest system sizes with odd L. In Figs. 5(a) and 5(b) we show how $|\varepsilon|$ depends on the many-body interaction V and the superconducting order parameter Δ for $\mu = 0$. Figures 5(c) and 5(d) show the same quantity for $\Delta = 0.6$ as a function of the many-body interaction V and chemical potential μ. Tuning the superconducting order parameter or the interaction strength is (most likely) not relevant for realistic experimental setups. Therefore, the most important result is that ε may be well tuned via changing the chemical potential.

E. Spatial structure of overlapping Majorana fermions after braiding

In order to follow the spatial structure of the overlapping Majorana fermions (Γ_1 and Γ_2) during a single adiabatic braiding on a single junction J_{12}, we represent both fermions as a linear combination of the local Majorana operators $\gamma_i^+ = a_i + a_i^\dagger$ and $\gamma_i^- = i(a_i - a_i^\dagger)$, namely, $\Gamma_m = \sum_i^L (\alpha_i^{m,+}\gamma_i^+ + \alpha_i^{m,-}\gamma_i^-)$ for $m \in \{1, 2\}$. Then, we apply the algorithm developed in Ref. [63] to find the coefficients $\alpha_i^{m,\pm}$ for each instantaneous Hamiltonian $H(t)$. This algorithm targets the MZMs following their formal definition via the commutation relations [6]: $\{\Gamma_m, \Gamma_{m'}\} = 2\delta_{m,m'}$ and $[\Gamma_m, H] = 0$. The latter commutation relations are invariant under the rotation $\vec{\Gamma} \rightarrow$

$\mathcal{O}(\beta)\vec{\Gamma}$, where

$$\vec{\Gamma} = \begin{bmatrix} \Gamma_1 \\ \Gamma_2 \end{bmatrix}, \quad \mathcal{O}(\beta) = \begin{bmatrix} \cos\beta & -\sin\beta \\ \sin\beta & \cos\beta \end{bmatrix}; \quad (20)$$

hence, also the coefficients $\alpha_i^{m,\pm}$ are defined up to an arbitrary choice of β. Initially, at time $t = t_0$, we choose the angle $\beta(t_0)$ following the standard convention in that Γ_1 and Γ_2 are located at the opposite edges of the trijunction, as shown in Fig. 4(c). Then, for each time t_j during the adiabatic evolution, we find the $\beta(t_j)$ that minimizes the (squared) distance,

$$\|\vec{\Gamma}(t_j) - \vec{\Gamma}(t_{j-1})\|^2 = \sum_{i=1}^{L} \sum_{m=1}^{2} \sum_{s=\pm} \left[\alpha_i^{m,s}(t_j) - \alpha_i^{m,s}(t_{j-1}) \right]^2. \quad (21)$$

If Majorana fermions are strict zero modes, then this approach reproduces the standard braiding that swaps the MZMs, i.e., $\Gamma_1(T) = \pm\Gamma_2(0)$ and $\Gamma_2(T) = \mp\Gamma_1(0)$. The latter swapping may also be written as $\vec{\Gamma}(T) = \mathcal{O}(\Delta\phi_{\text{Berry}})\vec{\Gamma}(0)$ for $\Delta\phi_{\text{Berry}} = \pm\frac{\pi}{2}$. It turns out that the latter relation holds true also for $\Delta\phi_{\text{Berry}} \neq \pm\frac{\pi}{2}$, i.e., also for braiding of the overlapping Majorana fermions. Then, however, the cyclic evolution cannot be understood as a simple swapping of the Majorana fermions. In particular $\Gamma_1(T)$ becomes a linear combination of both $\Gamma_1(0)$ and $\Gamma_2(0)$; hence, it contains nonvanishing contributions located at both edges of the junction [see Figs. 4(c)–4(d)]. The latter holds true whenever $\Delta\phi_{\text{Berry}}$ is not a multiple of $\pm\frac{\pi}{2}$.

F. Phase gate constructed from the braiding error

It is desirable to have a single junction on which one may perform the topologically protected operations, e.g., braiding of separated MZMs with $\Delta\phi_{\text{Berry}} = \pm\frac{\pi}{2}$, and also the unprotected adiabatic operations, e.g., the braiding of overlapping MZMs with $\Delta\phi_{\text{Berry}} \neq \pm\frac{\pi}{2}$. Due to the former operations, the trijunction with L sites should be as large as possible (formally, $L \to \infty$), and the corresponding protocol is schematically shown in Fig. 2(a). Then, in order to perform also the latter operation, one needs to bring both MZMs towards the center of the junction, so they start to overlap. This may be achieved via appropriate tuning of $\mu_i(t)$ in the time window $t \in (-\tau, 0)$ [see the left shaded area in Fig. 6(a)
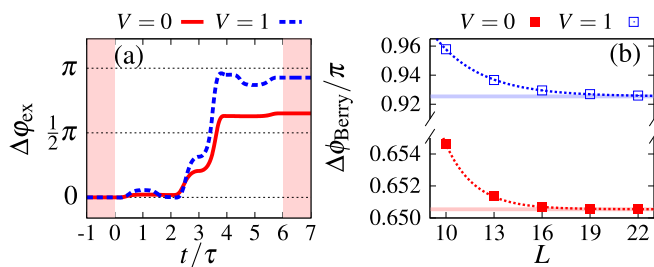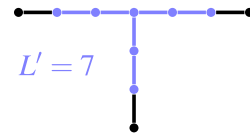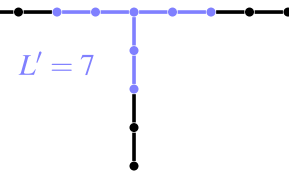
FIG. 6. Braiding of MZMs which are brought together for $t \in (-\tau, 0)$ and shifted apart for $t \in (6\tau, 7\tau)$. We set $\Delta = 0.8$, $\mu = 0$. (a) Exchange phase $\Delta\varphi_{\text{ex}}$ for $L = 19$ and $L' = 7$. (b) Geometric phase $\Delta\phi_{\text{Berry}}$ for $L' = 7$ vs L. Horizontal lines in (b) show $\Delta\phi_{\text{Berry}}(\infty)$ for $L' = 7$ obtained from the finite-size scaling to $L \to \infty$ using an exponential fitting function $\Delta\phi_{\text{Berry}}(L) = a\exp(-bL) + \Delta\phi_{\text{Berry}}(\infty)$.
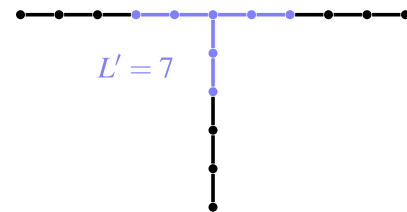
FIG. 7. A schematic plot of the unrestricted (all sites) and restricted (blue sites) junctions consisting of L and L' sites, respectively. Initially, two MZMs are located at the edges of the unrestricted junction. Then, they are brought together to the edges of the restricted junction, braided, and shifted apart to the initial positions at the edges of the unrestricted junction.

as well as Fig. 7]. Then, one may carry out the braiding protocol on the restricted trijunction with $L' \ll L$ sites in the time window $t \in (0, 6\tau)$. The latter protocol is sketched in Fig. 2(b). Finally, for $t \in (6\tau, 7\tau)$ the Majorana fermions are shifted apart to their original positions at the edges of the unrestricted (infinite) junction with L sites [see the right shaded area in Figs. 6(a) and 7].

Figure 6(a) shows the exchange phase $\Delta\varphi_{\text{ex}}(t)$ for $L = 19$ and $L' = 7$. The changes in $\Delta\varphi_{\text{ex}}(t)$ during the time windows when MZMs are brought together, $(-\tau, 0)$, or when they are shifted apart, $(6\tau, 7\tau)$, are small but not negligible. As discussed in Sec. III C, implementation of the phase gate depends on the braiding error ε; hence, the latter quantity should be finite also for $L \to \infty$. The most desirable scenario is when ε is determined mostly by L' and weakly depends on L. In order to establish the L dependence of the geometric phase we numerically studied the series of junctions shown in Fig. 7. Figure 6(b) shows one of the main results of the present work: the finite-size scaling of the geometric phase $\Delta\phi_{\text{Berry}}$ for fixed $L' = 7$ and various L. In contrast to results in Fig. 3(a), the braiding error is not a finite-size effect and remains nonzero also for $L \to \infty$ provided that L' is finite and Majorana fermions overlap during the braiding protocol. Weak L dependence of $\Delta\phi_{\text{Berry}}$ in Fig. 6(b) may originate from the leakage of MZMs into these sites, which remain in the trivial regime [13,83,84].

A robust scheme for obtaining a Majorana phase gate was recently discussed in Ref. [47] within an effective model that describes only MZMs, and the braiding was performed via changing the couplings between them in a specific time sequence. In the present case, these effective couplings arise from the parameters of the microscopic Hamiltonian (1), and the braiding is implemented via the time dependence of the local potentials. Nevertheless, the main objective of both approaches is the same: to eliminate the dynamical phase and to implement the phase gate in terms of the geometric phases. Repeating a specific gate protocol in Ref. [47] allows us to eliminate the dynamical phase and up to errors from the temporal change of the system between the parity-echo protocol steps. In the present approach the dynamical phase is eliminated due to the particle-hole symmetry of the system that hosts MZMs.

To summarize the discussion, in Fig. 2 we show a minimal setup for a single-qubit realization of all basic gates. In Figs. 2(a) and 2(c) we recall the standard implementations of the topologically protected gates $X = \begin{bmatrix} 0 & 1 \\ 1 & 0 \end{bmatrix}$ and $Z = \begin{bmatrix} 1 & 0 \\ 0 & -1 \end{bmatrix}$, respectively [45,85]. In both cases the MZMs do not overlap with each other throughout the entire protocol. In Fig. 2(b) we present the protocol for the phase gate $R(\theta)$, implemented via braiding of the overlapping MZMs.

IV. CONCLUSIONS

We have studied the dynamics of a qubit built out of four Majorana quasiparticles evolving on two trijunctions. We
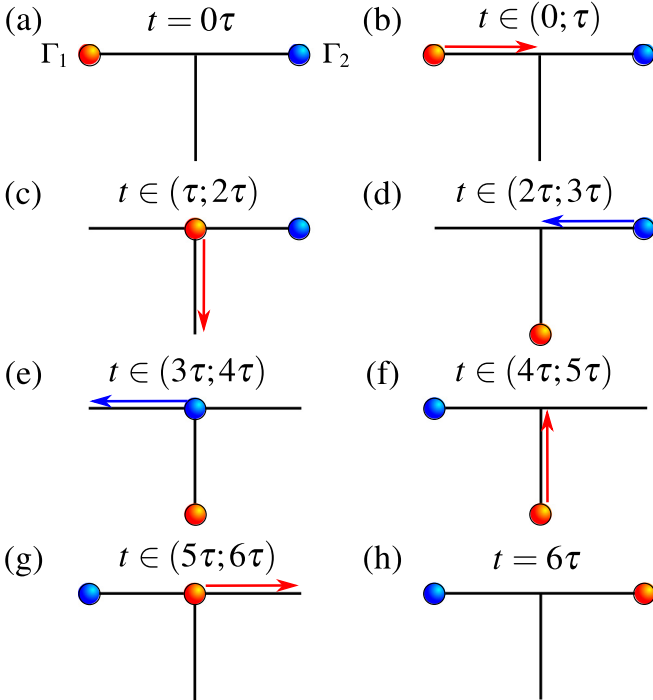

FIG. 8. Braiding protocol: (a) initial position of the MZMs, (b) moving Γ_1 to the center of the junction, (c) moving Γ_1 to the edge of the vertical chain, (d) moving Γ_2 to the center of the junction, (e) moving Γ_2 to the edge of the left chain, (f) moving Γ_1 to the center of the junction, (g) moving Γ_1 to the edge of the right chain, and (h) the final position of the MZMs.
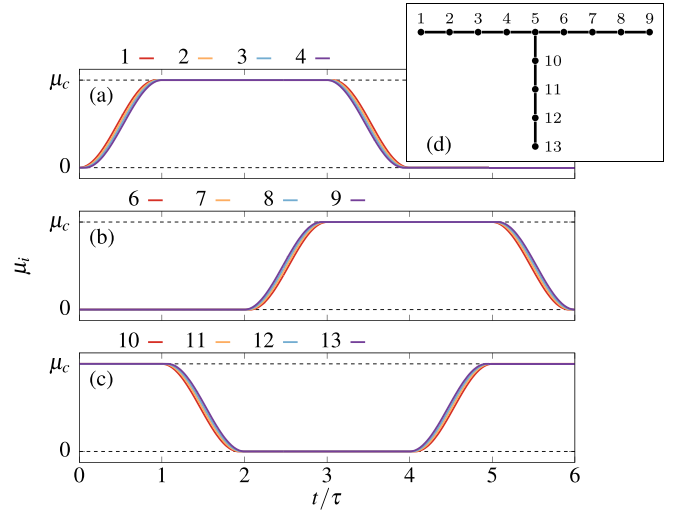

FIG. 9. Standard braiding protocol. (a)–(c) Potentials μ_i as a function of time t/τ in: (a) left, (b) right, and (c) vertical chains of the trijunction. (d) The numbering of sites.

focused on a case in which Majorana fermions evolve on spatially restricted junctions. Due to their mutual overlapping, they are not strict zero modes anymore; hence, the qubit acquires both dynamical and geometric phases during the braiding protocol. We have demonstrated that the dynamical contribution may be canceled out if the trijunctions are described by the same particle-hole-symmetric Hamiltonian and contain an odd number of the lattice sites. The geometric contribution deviates from that for braiding of strict zero modes $\Delta\phi_{\text{Berry}} = \pm\frac{\pi}{2}$, and the latter deviation allows one to build the adiabatic phase gate with tunable phase shift. The
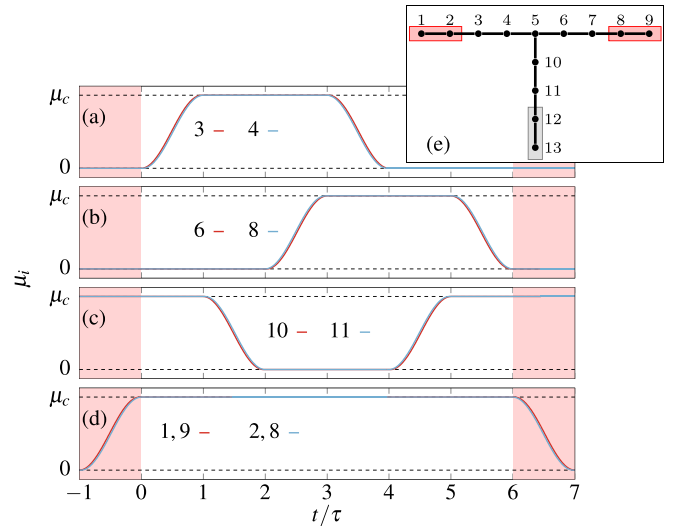

FIG. 10. Extended braiding protocol in which MZMs are brought together for $t \in (-\tau, 0)$ and shifted apart for $t \in (6\tau, 7\tau)$. (a)–(d) Potentials μ_i as a function of time t/τ for selected sites of (a) left, (b) right, and (c) vertical chains of the trijunction, which is schematically represented in (e); (d) shows μ_i for sites marked with red rectangles in (e). For sites which are marked with the gray rectangle in (e) we set $\mu_i(t) = \mu_c$ throughout the protocol.

only difference with respect to the topologically protected braiding of MZMs consists of the fact that the Majorana fermions are brought together before the braiding and are shifted apart after the braiding. Probably, the protocol still should be followed by some error correction; however, the initial error is expected to be smaller than in the standard protocol based on the dynamical phase.

APPENDIX: SMOOTH RAMPING PROTOCOL

We use exactly the same smooth ramping protocol as in Ref. [53]. Figure 8 illustrates subsequent steps of the braiding protocol and the corresponding time windows. The swap of MZMs is achieved via appropriate tuning of $\mu_i(t)$; see Eqs. (1) and (2) in the main text. Whenever we ramp up selected sites, we use the following time-dependent function $g_i(t) \in [0, 1]$:

$$g_i(t) = m\left\{\frac{t}{\tau}[1 + \alpha(\ell - 1)] - \alpha(\ell - i)\right\}, \quad t \in [0, \tau],$$
(A1)

where we take $\alpha = 0.025$ and ℓ is the length of each chain, i.e., $L = 3\ell + 1$. Here, $m(x)$ is a scalar function, $m(x) = \sin^2[\frac{\pi}{2}r(x)]$, and $r(x)$ is a linear ramp, $r(x) = \min[\max(x, 0), 1]$. For the ramp-down protocol, we replace $t \rightarrow \tau - t$ in Eq. (A1) to reverse the process in time. Figure 9 shows $\mu_i(t)$ for the standard braiding protocol relevant for Fig. 3 in the main text. Figure 10 shows the same, but for the extended protocol in which MZMs are first brought together for $t \in (-\tau, 0)$, braided for $t \in (0, 6\tau)$, and shifted apart for $t \in (6\tau, 7\tau)$; see Fig. 6 in the main text.

[1] D. A. Ivanov, Non-Abelian Statistics of Half-Quantum Vortices in *p*-Wave Superconductors, Phys. Rev. Lett. **86**, 268 (2001).

[2] S. Das Sarma, M. Freedman, and C. Nayak, Topologically Protected Qubits from a Possible Non-Abelian Fractional Quantum Hall State, Phys. Rev. Lett. **94**, 166802 (2005).

[3] P. Bonderson, M. Freedman, and C. Nayak, Measurement-Only Topological Quantum Computation, Phys. Rev. Lett. **101**, 010501 (2008).

[4] C. Nayak, S. H. Simon, A. Stern, M. Freedman, and S. Das Sarma, Non-Abelian anyons and topological quantum computation, Rev. Mod. Phys. **80**, 1083 (2008).

[5] A. R. Akhmerov, Topological quantum computation away from the ground state using Majorana fermions, Phys. Rev. B **82**, 020509(R) (2010).

[6] S. Das Sarma, M. Freedman, and C. Nayak, Majorana zero modes and topological quantum computation, npj Quantum Inf. **1**, 15001 (2015).

[7] S. Plugge, L. A. Landau, E. Sela, A. Altland, K. Flensberg, and R. Egger, Roadmap to Majorana surface codes, Phys. Rev. B **94**, 174514 (2016).

[8] D. Aasen, M. Hell, R. V. Mishmash, A. Higginbotham, J. Danon, M. Leijnse, T. S. Jespersen, J. A. Folk, C. M. Marcus, K. Flensberg, and J. Alicea, Milestones Toward Majorana-Based Quantum Computing, Phys. Rev. X **6**, 031016 (2016).

[9] T. Karzig, C. Knapp, R. M. Lutchyn, P. Bonderson, M. B. Hastings, C. Nayak, J. Alicea, K. Flensberg, S. Plugge, Y. Oreg, C. M. Marcus, and M. H. Freedman, Scalable designs for quasiparticle-poisoning-protected topological quantum computation with Majorana zero modes, Phys. Rev. B **95**, 235305 (2017).

[10] R. Aguado, Majorana quasiparticles in condensed matter, Riv. Nuovo Cimento **40**, 523 (2017).

[11] R. M. Lutchyn, E. P. A. M. Bakkers, L. P. Kouwenhoven, P. Krogstrup, C. M. Marcus, and Y. Oreg, Majorana zero modes in superconductor–semiconductor heterostructures, Nat. Rev. Mater. **3**, 52 (2018).

[12] D. Sticlet, C. Bena, and P. Simon, Spin and Majorana Polarization in Topological Superconducting Wires, Phys. Rev. Lett. **108**, 096802 (2012).

[13] A. Ptok, A. Kobiałka, and T. Domański, Controlling the bound states in a quantum-dot hybrid nanowire, Phys. Rev. B **96**, 195430 (2017).

[14] M. M. Maśka and T. Domański, Polarization of the Majorana quasiparticles in the Rashba chain, Sci. Rep. **7**, 16193 (2017).

[15] M. M. Maśka, A. Gorczyca-Goraj, J. Tworzydło, and T. Domański, Majorana quasiparticles of an inhomogeneous Rashba chain, Phys. Rev. B **95**, 045429 (2017).

[16] J. Li, S. Jeon, Y. Xie, A. Yazdani, and B. A. Bernevig, Majorana spin in magnetic atomic chain systems, Phys. Rev. B **97**, 125119 (2018).

[17] A. Kobiałka, T. Domański, and A. Ptok, Delocalisation of Majorana quasiparticles in plaquette–nanowire hybrid system, Sci. Rep. **9**, 12933 (2019).

[18] A. Kobiałka and A. Ptok, Electrostatic formation of the Majorana quasiparticles in the quantum dot-nanoring structure, J. Phys.: Condens. Matter **31**, 185302 (2019).

[19] C.-X. Liu, J. D. Sau, T. D. Stanescu, and S. Das Sarma, Andreev bound states versus Majorana bound states in quantum dot-nanowire-superconductor hybrid structures: Trivial versus topological zero-bias conductance peaks, Phys. Rev. B **96**, 075161 (2017).

[20] C.-X. Liu, J. D. Sau, and S. Das Sarma, Distinguishing topological Majorana bound states from trivial Andreev bound states: Proposed tests through differential tunneling conductance spectroscopy, Phys. Rev. B **97**, 214502 (2018).

[21] M. Hell, K. Flensberg, and M. Leijnse, Distinguishing Majorana bound states from localized Andreev bound states by interferometry, Phys. Rev. B **97**, 161401(R) (2018).

[22] M. T. Deng, C. L. Yu, G. Y. Huang, M. Larsson, P. Caroff, and H. Q. Xu, Anomalous zero-bias conductance peak in a Nb–InSb nanowire–Nb hybrid device, Nano Lett. **12**, 6414 (2012).

[23] V. Mourik, K. Zuo, S. M. Frolov, S. R. Plissard, E. P. A. M. Bakkers, and L. P. Kouwenhoven, Signatures of Majorana fermions in hybrid superconductor-semiconductor nanowire devices, Science **336**, 1003 (2012).

[24] A. Das, Y. Ronen, Y. Most, Y. Oreg, M. Heiblum, and H. Shtrikman, Zero-bias peaks and splitting in an Al-InAs nanowire topological superconductor as a signature of Majorana fermions, Nat. Phys. **8**, 887 (2012).

[25] A. D. K. Finck, D. J. Van Harlingen, P. K. Mohseni, K. Jung, and X. Li, Anomalous Modulation of a Zero-Bias Peak in a Hybrid Nanowire-Superconductor Device, Phys. Rev. Lett. **110**, 126406 (2013).

[26] F. Nichele, A. C. C. Drachmann, A. M. Whiticar, E. C. T. O'Farrell, H. J. Suominen, A. Fornieri, T. Wang, G. C. Gardner, C. Thomas, A. T. Hatke, P. Krogstrup, M. J. Manfra, K. Flensberg, and C. M. Marcus, Scaling of Majorana Zero-Bias Conductance Peaks, Phys. Rev. Lett. **119**, 136803 (2017).

[27] Ö. Gül, H. Zhang, J. D. S. Bommer, M. W. A. de Moor, D. Car, S. R. Plissard, E. P. A. M. Bakkers, A. Geresdi, K. Watanabe, T. Taniguchi, and L. P. Kouwenhoven, Ballistic Majorana nanowire devices, Nat. Nanotechnol. **13**, 192 (2018).

[28] M. T. Deng, S. Vaitiekėnas, E. B. Hansen, J. Danon, M. Leijnse, K. Flensberg, J. Nygård, P. Krogstrup, and C. M. Marcus, Majorana bound state in a coupled quantum-dot hybrid-nanowire system, Science **354**, 1557 (2016).

[29] M.-T. Deng, S. Vaitiekėnas, E. Prada, P. San-Jose, J. Nygård, P. Krogstrup, R. Aguado, and C. M. Marcus, Nonlocality of Majorana modes in hybrid nanowires, Phys. Rev. B **98**, 085125 (2018).

[30] H. Zhang, C.-X. Liu, S. Gazibegovic, D. Xu, J. A. Logan, G. Wang, N. Van Loo, J. D. Bommer, M. W. De Moor, D. Car *et al.*, Quantized Majorana conductance, Nature (London) **556**, 74 (2018).

[31] D. Wang, L. Kong, P. Fan, H. Chen, S. Zhu, W. Liu, L. Cao, Y. Sun, S. Du, J. Schneeloch, R. Zhong, G. Gu, L. Fu, H. Ding, and H.-J. Gao, Evidence for Majorana bound states in an iron-based superconductor, Science **362**, 333 (2018).

[32] S. Nadj-Perge, I. K. Drozdov, J. Li, H. Chen, S. Jeon, J. Seo, A. H. MacDonald, B. A. Bernevig, and A. Yazdani, Observation of Majorana fermions in ferromagnetic atomic chains on a superconductor, Science **346**, 602 (2014).

[33] R. Pawlak, M. Kisiel, J. Klinovaja, T. Meier, S. Kawai, T. Glatzel, D. Loss, and E. Meyer, Probing atomic structure and Majorana wavefunctions in mono-atomic Fe chains on superconducting Pb surface, npj Quantum Inf. **2**, 16035 (2016).

[34] B. E. Feldman, M. T. Randeria, J. Li, S. Jeon, Y. Xie, Z. Wang, I. K. Drozdov, B. A. Bernevig, and A. Yazdani, High-resolution studies of the Majorana atomic chain platform, Nat. Phys. **13**, 286 (2016).

[35] M. Ruby, B. W. Heinrich, Y. Peng, F. von Oppen, and K. J. Franke, Exploring a proximity-coupled Co chain on Pb(110) as a possible Majorana platform, Nano Lett. **17**, 4473 (2017).

[36] S. Jeon, Y. Xie, J. Li, Z. Wang, B. A. Bernevig, and A. Yazdani, Distinguishing a Majorana zero mode using spin-resolved measurements, Science **358**, 772 (2017).

[37] H. Kim, A. Palacio-Morales, T. Posske, L. Rózsa, K. Palotás, L. Szunyogh, M. Thorwart, and R. Wiesendanger, Toward tailoring Majorana bound states in artificially constructed magnetic atom chains on elemental superconductors, Sci. Adv. **4**, eaar5251 (2018).

[38] H.-H. Sun and J.-F. Jia, Detection of Majorana zero mode in the vortex, npj Quantum Mater. **2**, 34 (2017).

[39] T. Machida, Y. Sun, S. Pyon, S. Takeda, Y. Kohsaka, T. Hanaguri, T. Sasagawa, and T. Tamegai, Zero-energy vortex bound state in the superconducting topological surface state of Fe(Se,Te), Nat. Mater. **18**, 811 (2019).

[40] K. Jiang, X. Dai, and Z. Wang, Quantum Anomalous Vortex and Majorana Zero Mode in Iron-Based Superconductor Fe(Te,Se), Phys. Rev. X **9**, 011033 (2019).

[41] C.-K. Chiu, T. Machida, Y. Huang, T. Hanaguri, and F.-C. Zhang, Scalable Majorana vortex modes in iron-based superconductors, arXiv:1904.13374.

[42] G. C. Ménard, S. Guissart, C. Brun, R. T. Leriche, M. Trif, F. Debontridder, D. Demaille, D. Roditchev, P. Simon, and T. Cren, Two-dimensional topological superconductivity in Pb/Co/Si(111), Nat. Commun. **8**, 2040 (2017).

[43] A. Palacio-Morales, E. Mascot, S. Cocklin, H. Kim, S. Rachel, D. K. Morr, and R. Wiesendanger, Atomic-scale interface engineering of Majorana edge modes in a 2D magnet-superconductor hybrid system, Sci. Adv. **5**, eaav6600 (2019).

[44] M. A. Nielsen and I. L. Chuang, *Quantum Computation and Quantum Information*, 10th anniversary ed. (Cambridge University Press, New York, 2011).

[45] J. Alicea, Y. Oreg, G. Refael, F. Von Oppen, and M. P. Fisher, Non-Abelian statistics and topological quantum information processing in 1D wire networks, Nat. Phys. **7**, 412 (2011).

[46] B. van Heck, A. R. Akhmerov, F. Hassler, M. Burrello, and C. W. J. Beenakker, Coulomb-assisted braiding of Majorana fermions in a Josephson junction array, New J. Phys. **14**, 035019 (2012).

[47] T. Karzig, Y. Oreg, G. Refael, and M. H. Freedman, Universal Geometric Path to a Robust Majorana Magic Gate, Phys. Rev. X **6**, 031019 (2016).

[48] L.-H. Wu, Q.-F. Liang, and X. Hu, New scheme for braiding Majorana fermions, Sci. Technol. Adv. Mater. **15**, 064402 (2014).

[49] F. L. Pedrocchi and D. P. DiVincenzo, Majorana Braiding with Thermal Noise, Phys. Rev. Lett. **115**, 120402 (2015).

[50] Q.-B. Cheng, J. He, and S.-P. Kou, Verifying non-Abelian statistics by numerical braiding Majorana fermions, Phys. Lett. A **380**, 779 (2016).

[51] J. Li, T. Neupert, B. A. Bernevig, and A. Yazdani, Manipulating Majorana zero modes on atomic rings with an external magnetic field, Nat. Commun. **7**, 10395 (2016).

[52] A. Matos-Abiague, J. Shabani, A. D. Kent, G. L. Fatin, B. Scharf, and I. Žutić, Tunable magnetic textures: From Majorana bound states to braiding, Solid State Commun. **262**, 1 (2017).

[53] M. Sekania, S. Plugge, M. Greiter, R. Thomale, and P. Schmitteckert, Braiding errors in interacting Majorana quantum wires, Phys. Rev. B **96**, 094307 (2017).

[54] B. Bauer, T. Karzig, R. V. Mishmash, A. E. Antipov, and J. Alicea, Dynamics of Majorana-based qubits operated with an array of tunable gates, SciPost Phys. **5**, 004 (2018).

[55] K. Ritland and A. Rahmani, Optimal noise-canceling shortcuts to adiabaticity: Application to noisy Majorana-based gates, New J. Phys. **20**, 065005 (2018).

[56] C. Malciu, L. Mazza, and C. Mora, Braiding Majorana zero modes using quantum dots, Phys. Rev. B **98**, 165426 (2018).

[57] S. Bravyi and A. Kitaev, Universal quantum computation with ideal Clifford gates and noisy ancillas, Phys. Rev. A **71**, 022316 (2005).

[58] A. Y. Kitaev, Unpaired Majorana fermions in quantum wires, Phys. Usp. **44**, 131 (2001).

[59] F. D. M. Haldane, 'Luttinger liquid theory' of one-dimensional quantum fluids. I. Properties of the Luttinger model and their extension to the general 1D interacting spinless Fermi gas, J. Phys. C **14**, 2585 (1981).

[60] S. Gangadharaiah, B. Braunecker, P. Simon, and D. Loss, Majorana Edge States in Interacting One-Dimensional Systems, Phys. Rev. Lett. **107**, 036801 (2011).

[61] A. Manolescu, D. C. Marinescu, and T. D. Stanescu, Coulomb interaction effects on the Majorana states in quantum wires, J. Phys.: Condens. Matter **26**, 172203 (2014).

[62] R. Thomale, S. Rachel, and P. Schmitteckert, Tunneling spectra simulation of interacting Majorana wires, Phys. Rev. B **88**, 161103(R) (2013).

[63] A. Więckowski, M. M. Maśka, and M. Mierzejewski, Identification of Majorana Modes in Interacting Systems by Local Integrals of Motion, Phys. Rev. Lett. **120**, 040504 (2018).

[64] Y. Peng, F. Pientka, L. I. Glazman, and F. von Oppen, Strong Localization of Majorana End States in Chains of Magnetic Adatoms, Phys. Rev. Lett. **114**, 106801 (2015).

[65] H. T. Ng, Decoherence of interacting Majorana modes, Sci. Rep. **5**, 12530 (2015).

[66] Y.-H. Chan, C.-K. Chiu, and K. Sun, Multiple signatures of topological transitions for interacting fermions in chain lattices, Phys. Rev. B **92**, 104514 (2015).

[67] J. S. Hofmann, F. F. Assaad, and A. P. Schnyder, Edge instabilities of topological superconductors, Phys. Rev. B **93**, 201116(R) (2016).

[68] F. Domínguez, J. Cayao, P. San-Jose, R. Aguado, A. L. Yeyati, and E. Prada, Zero-energy pinning from interactions in Majorana nanowires, npj Quantum Mater. **2**, 13 (2017).

[69] E. M. Stoudenmire, J. Alicea, O. A. Starykh, and M. P. A. Fisher, Interaction effects in topological superconducting wires supporting Majorana fermions, Phys. Rev. B **84**, 014503 (2011).

[70] N. M. Gergs, L. Fritz, and D. Schuricht, Topological order in the Kitaev/Majorana chain in the presence of disorder and interactions, Phys. Rev. B **93**, 075129 (2016).

[71] F. Hassler and D. Schuricht, Strongly interacting Majorana modes in an array of Josephson junctions, New J. Phys. **14**, 125018 (2012).

[72] J. Alicea, New directions in the pursuit of Majorana fermions in solid state systems, Rep. Prog. Phys. **75**, 076501 (2012).

[73] H. Katsura, D. Schuricht, and M. Takahashi, Exact ground states and topological order in interacting Kitaev/Majorana chains, Phys. Rev. B **92**, 115137 (2015).

[74] G. Torres-Vega, Chebyshev scheme for the propagation of quantum wave functions in phase space, J. Chem. Phys. **99**, 1824 (1993).

[75] H. Fehske, J. Schleede, G. Schubert, G. Wellein, V. S. Filinov, and A. R. Bishop, Numerical approaches to time evolution of complex quantum systems, Phys. Lett. A **373**, 2182 (2009).

[76] A. Alvermann, H. Fehske, and P. B. Littlewood, Numerical time propagation of quantum systems in radiation fields, New J. Phys. **14**, 105008 (2012).

[77] M. V. Berry, Quantal phase factors accompanying adiabatic changes, Proc. R. Soc. London, Ser. A **392**, 45 (1983).

[78] Y. Aharonov and J. Anandan, Phase Change During a Cyclic Quantum Evolution, Phys. Rev. Lett. **58**, 1593 (1987).

[79] J. Anandan, J. Christian, and K. Wanelik, Resource letter GPP-1: Geometric phases in physics, Am. J. Phys. **65**, 180 (1997).

[80] N. Mukunda and R. Simon, Quantum kinematic approach to the geometric phase. I. General formalism, Ann. Phys. (NY) **228**, 205 (1993).

[81] M. Ezawa, Non-Abelian braiding of Majorana-like edge states and scalable topological quantum computations in electric circuits, arXiv:1907.06911.

[82] F. H. L. Essler, H. Frahm, F. Göhmann, A. Klümper, and V. E. Korepin, *The One-Dimensional Hubbard Model* (Cambridge University Press, Cambridge, 2005).

[83] J. Klinovaja and D. Loss, Composite Majorana fermion wave functions in nanowires, Phys. Rev. B **86**, 085408 (2012).

[84] D. A. Ruiz-Tijerina, E. Vernek, L. G. G. V. Dias da Silva, and J. C. Egues, Interaction effects on a Majorana zero mode leaking into a quantum dot, Phys. Rev. B **91**, 115435 (2015).

[85] S. Bravyi, Universal quantum computation with the $\nu = 5/2$ fractional quantum hall state, Phys. Rev. A **73**, 042313 (2006).